Article

Cell Reports

Brain State Dependence of Hippocampal Subthreshold Activity in Awake Mice

Graphical Abstract

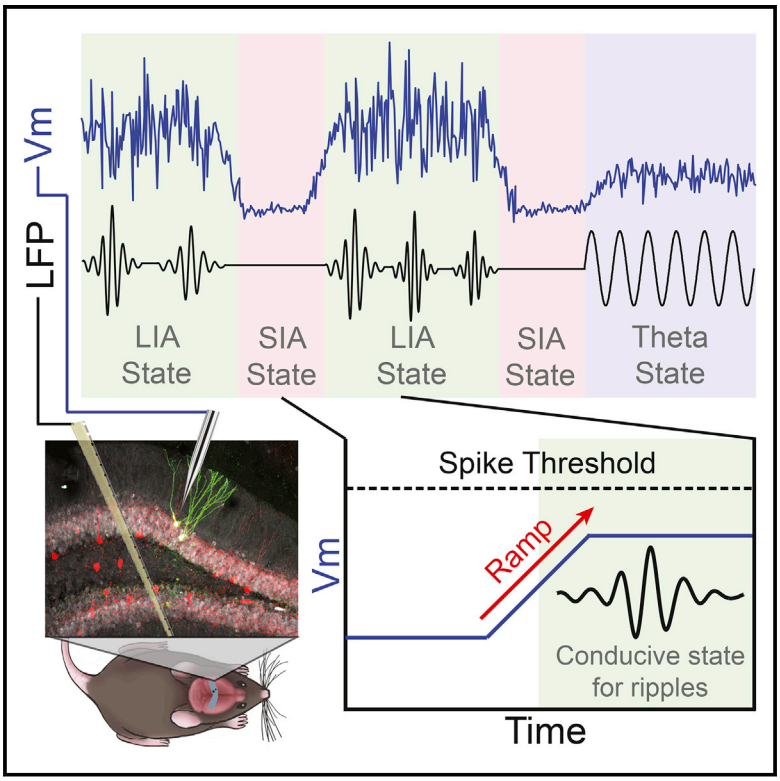

Authors

Brad K. Hulse, Evgueniy V. Lubenov, Athanassios G. Siapas

Correspondence

thanos@caltech.edu

In Brief

Hulse et al. show that the average membrane potential and the amplitude of subthreshold fluctuations of hippocampal neurons systematically change with brain state and arousal. This results in membrane potential ramps that precede ripples and mirror transitions to a network regime conducive for ripple generation.

Highlights

- Combined intracellular and extracellular recordings of awake hippocampal activity
- Hippocampal membrane potential statistics are brain state dependent
- Rapid fluctuations in arousal are mirrored in hippocampal subthreshold activity
- Ramps in the membrane potential of hippocampal neurons precede ripple onset

Hulse et al., 2017, Cell Reports *18*, 136–147
January 3, 2017
http://dx.doi.org/10.1016/j.celrep.2016.11.084

OPEN ACCESS
CellPress

Cell Reports
Article

Brain State Dependence of Hippocampal Subthreshold Activity in Awake Mice

Brad K. Hulse,[1] Evgueniy V. Lubenov,[1] and Athanassios G. Siapas[1,2,3,4,*]
[1]Division of Biology and Biological Engineering
[2]Division of Engineering and Applied Science
[3]Computation and Neural Systems Program
California Institute of Technology, 1200 East California Blvd., Pasadena, CA 91125, USA
[4]Lead Contact
*Correspondence: thanos@caltech.edu
http://dx.doi.org/10.1016/j.celrep.2016.11.084

SUMMARY

Monitoring the membrane potential of individual neurons has uncovered how single-cell properties contribute to network processing across different brain states in neocortex. In contrast, the subthreshold modulation of hippocampal neurons by brain state has not been systematically characterized. To address this, we combined whole-cell recordings from dentate granule cells and CA1 pyramidal neurons with multisite extracellular recordings and behavioral measurements in awake mice. We show that the average membrane potential, amplitude of subthreshold fluctuations, and distance to spike threshold are all modulated by brain state. Furthermore, even within individual states, rapid variations in arousal are reflected in membrane potential fluctuations. These factors produce depolarizing ramps in the membrane potential of hippocampal neurons that precede ripples and mirror transitions to a network regime conducive for ripple generation. These results suggest that there are coordinated shifts in the subthreshold dynamics of individual neurons that underlie the transitions between distinct modes of hippocampal processing.

INTRODUCTION

The hippocampus plays a critical role in spatial navigation and the encoding, consolidation, and retrieval of new episodic memories (Squire, 1992). Importantly, distinct brain states are thought to contribute differentially to each process. Because of this, state-dependent patterns of spiking and local field potential (LFP) oscillations have been studied extensively in the hippocampal formation (Vanderwolf, 1969, 1971; O'Keefe and Nadel, 1978; Buzsáki et al., 1983, 1992; Wilson and McNaughton, 1994; Lubenov and Siapas, 2009; Kay et al., 2016; Shan et al., 2016). During wakefulness, periods of locomotion are associated with robust theta (5–12 Hz) and gamma (30–80 Hz) oscillations in the LFP. In this state, individual principal neurons, known as place cells, fire at particular spatial locations and are largely silent otherwise (O'Keefe, 1976). It has been hypothesized that memory encoding preferentially occurs during this state (Buzsáki, 1989). During periods of low arousal, the hippocampal LFP is characterized by large irregular activity (LIA), during which trains of sharp waves often co-occur with high-frequency (80–250 Hz) ripple oscillations (Vanderwolf, 1969; O'Keefe, 1976; Buzsáki, 1986). Sharp-wave/ripples (SWRs) are associated with population bursts that "replay" previously experienced spatial trajectories (Lee and Wilson, 2002; Foster and Wilson, 2006; Diba and Buzsáki, 2007). These replay events are hypothesized to contribute to the consolidation and retrieval of newly formed episodic memories (Carr et al., 2011). In addition to the theta and LIA states, a third state of intermediate arousal exists, during which LFPs show a decline in broadband power. This state is termed "small irregular activity" (SIA) (Vanderwolf, 1971; O'Keefe and Nadel, 1978; Jarosiewicz and Skaggs, 2004b; Kay et al., 2016), though other terms have also been used (Lapray et al., 2012; Katona et al., 2014). During periods of SIA, most principal cells stop firing, while a small subset fires robustly and may code for spatial position in the absence of locomotion (Jarosiewicz et al., 2002; Jarosiewicz and Skaggs, 2004b; Kay et al., 2016). In addition to principal cells, recent work also finds strong state-dependent firing patterns in identified hippocampal interneurons during LIA, SIA, and theta (Somogyi et al., 2013).

The ability of brain circuits to generate such distinct activity patterns has been hypothesized to rely upon state-dependent modulations in single-cell properties, such as the resting membrane potential, distance to spike threshold, and synaptic efficacy (Winson and Abzug, 1977; Getting, 1989; Hasselmo, 1999; Harris and Thiele, 2011; Lee and Dan, 2012; Marder, 2012; Marder et al., 2014). Despite this, the subthreshold modulation of hippocampal neurons by brain state has not been systematically characterized. Recent studies in neocortex have found rapid brain state changes in awake animals with behaviorally relevant effects on the spiking patterns and encoding abilities of sensory and motor regions (Niell and Stryker, 2010; Vyazovskiy et al., 2011; Reimer et al., 2014; McGinley et al., 2015b; Vinck et al., 2015). Importantly, intracellular recordings of subthreshold activity during behavior have been instrumental in elucidating the cellular mechanisms contributing to the emergence of these network activity patterns in neocortex (Steriade

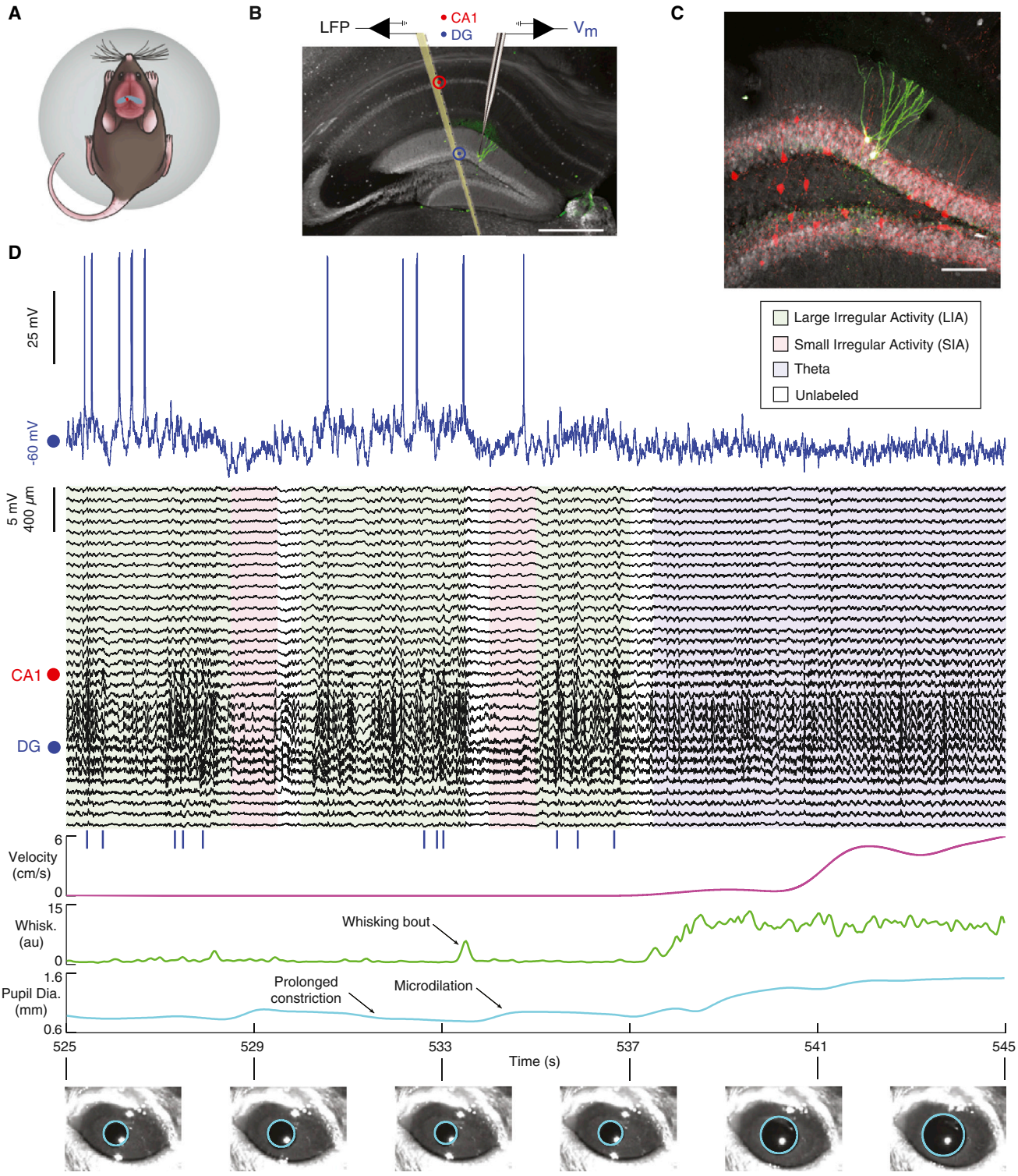

Figure 1. The Subthreshold Activity of Hippocampal Principal Cells Varies with Brain State in Awake Mice

(A) Schematic of a mouse on the spherical treadmill. The approximate whole-cell (red dot) and LFP (black dot) recording locations are marked over dorsal hippocampus (blue).

(B) Fluorescent image of a 100-μm-thick coronal section of dorsal hippocampus with two stained dentate granule cells (green) and immunohistochemistry against calbindin (gray) illustrating the placement of the multisite silicon probe and patch pipette. Scale bar, 500 μm.

(legend continued on next page)

et al., 2001; Poulet and Petersen, 2008; Polack et al., 2013; McGinley et al., 2015a; Schiemann et al., 2015). However, the nature of the observed effects depends on the neocortical area and cell type investigated, resulting in at least three distinct models of subthreshold modulation by arousal/state: the binary, sigmoidal, and U models (McGinley et al., 2015b). According to the binary and sigmoidal models, the membrane potential should depolarize with increasing arousal, as low-frequency (<10 Hz) activity is replaced by gamma oscillations. According to the U model, the membrane potential should be most hyperpolarized at intermediate levels of arousal, when low-frequency activity and gamma oscillations are minimal. Given the diversity of findings in neocortex, predicting how hippocampal subthreshold activity depends on brain state is difficult, underscoring the importance of this measurement. In addition, the circuit mechanisms underlying this state dependence in neocortex need not be the same as those in the hippocampus, which possesses its own characteristic architecture and neuromodulatory influences.

Furthermore, the impact of fluctuations in arousal within particular brain states on hippocampal network activity remains poorly understood. Previous neocortical studies in rodents have divided wakefulness into "quiet" and "active" periods based on the presence or absence of overt exploratory behavior, such as whisking and locomotion. However, such a coarse division may neglect functionally important network fluctuations occurring within states. Over the past 5 decades, primate studies have measured fluctuations in pupil diameter to track arousal-associated state changes during awake behavior (Hess and Polt, 1960, 1964; Wilhelm et al., 2001; Kristjansson et al., 2009; McGinley et al., 2015b). Similarly, a recent experiment in mouse neocortex found that, even within periods of quiet wakefulness, there exist fast fluctuations in arousal, assessed through pupillometry, that modulate neocortical subthreshold activity (Reimer et al., 2014). Together, these studies establish pupil diameter as a particularly important behavioral measurement, since it tracks changes in the mouse's level of arousal, even in the absence of overt exploratory behavior (Reimer et al., 2014, 2016; McGinley et al., 2015b; Vinck et al., 2015). However, whether fluctuations in pupil diameter during quiet wakefulness are mirrored in hippocampal subthreshold activity remains unknown.

Here, we performed in vivo whole-cell recordings of the membrane potential (Vm) from identified dentate granule cells and CA1 pyramidal neurons during LIA, SIA, and theta states in awake mice. Using this approach, we demonstrate that the membrane potential statistics (mean, variability, and distance to threshold) of hippocampal neurons are approximately U-shaped functions of arousal. In addition, we observe rapid fluctuations in pupil diameter within sustained periods of LIA that are reflected in subthreshold activity changes. Finally, many neurons exhibit ramps in the membrane potential starting approximately 1 s before ripples, reflecting transitions to a network regime conducive for ripple generation.

RESULTS

Differences in Membrane Potential Statistics across Brain States

To investigate how hippocampal subthreshold activity changes with brain state, we combined whole-cell recordings from identified dentate granule cells and CA1 pyramidal neurons with simultaneous LFP measurements from a nearby multisite silicon probe in awake, head-fixed mice that were free to walk on a spherical treadmill (Figures 1A–1C; Movie S1) (Hulse et al., 2016). Concurrently, the mouse's behavioral level of arousal was tracked by measuring locomotor velocity, whisking activity, and pupil diameter. LFP sites spanned neocortex, hippocampal area CA1 and the dentate gyrus (DG), and parts of the thalamus. We identified periods of wakefulness as LIA (37%), SIA (6%), or theta (6%) based on the spectral content of hippocampal LFPs, leaving the remaining 51% unlabeled (Figures S1 and S2B; see Experimental Procedures). The objective was to identify prototypical segments of sufficient duration as opposed to providing an exhaustive brain state assignment over the whole recording period. We then studied changes in subthreshold activity and behavior during transitions to and within periods of LIA, SIA, and theta.

Figure 1D shows an example whole-cell recording from a dentate granule cell with simultaneous LFP and behavioral measurements during a period with LIA, SIA, and theta. Notice that, during periods of LIA, the pupil is constricted (or constricting), whisking and locomotor activity are low, and the hippocampal LFP shows trains of large-amplitude sharp waves often co-occurring with high-frequency ripple oscillations in the CA1 pyramidal cell layer. The membrane potential appears depolarized and has large-amplitude fluctuations, occasionally exceeding spike threshold. In this example, LIA was interrupted by two brief (~1 s) periods of SIA that were associated with whisking bouts and a microdilation of the pupil. During these SIA epochs, the Vm appears hyperpolarized. The segment ends with a period of theta oscillations associated with locomotion, high whisking activity, and a dilated pupil. During this period, the membrane potential was at an intermediate level of depolarization and variability, compared to LIA and SIA. In order to investigate how general these trends were across neurons, we recorded dentate granule cells (n = 20) and CA1 pyramidal neurons (n = 31) across a total of 13.4 hr of spontaneous activity and studied the behavioral variables and Vm during transitions to LIA, SIA, and theta (Figures 2, 3, and S2).

(C) Confocal image from section in (B) showing the two biocytin-stained dentate granule cells (green) with combined immunohistochemistry against parvalbumin (red) and calbindin (gray). Scale bar, 100 μm.

(D) Example of simultaneous intracellular (blue), multisite LFP (black), locomotor velocity (magenta), whisking (Whisk.; green), and pupil diameter (Pupil Dia.; cyan) measurements during a period with LIA, SIA, and theta. The legend lists each state's coloring in the LFP plot below. The red dot marks the channel within the CA1 pyramidal cell layer showing LFP ripple oscillations. The blue dot marks an LFP channel in the DG. Blue vertical lines below LFPs indicate ripple occurrence. Example pupil fits are shown below.

See also Figure S1 and Movie S1.

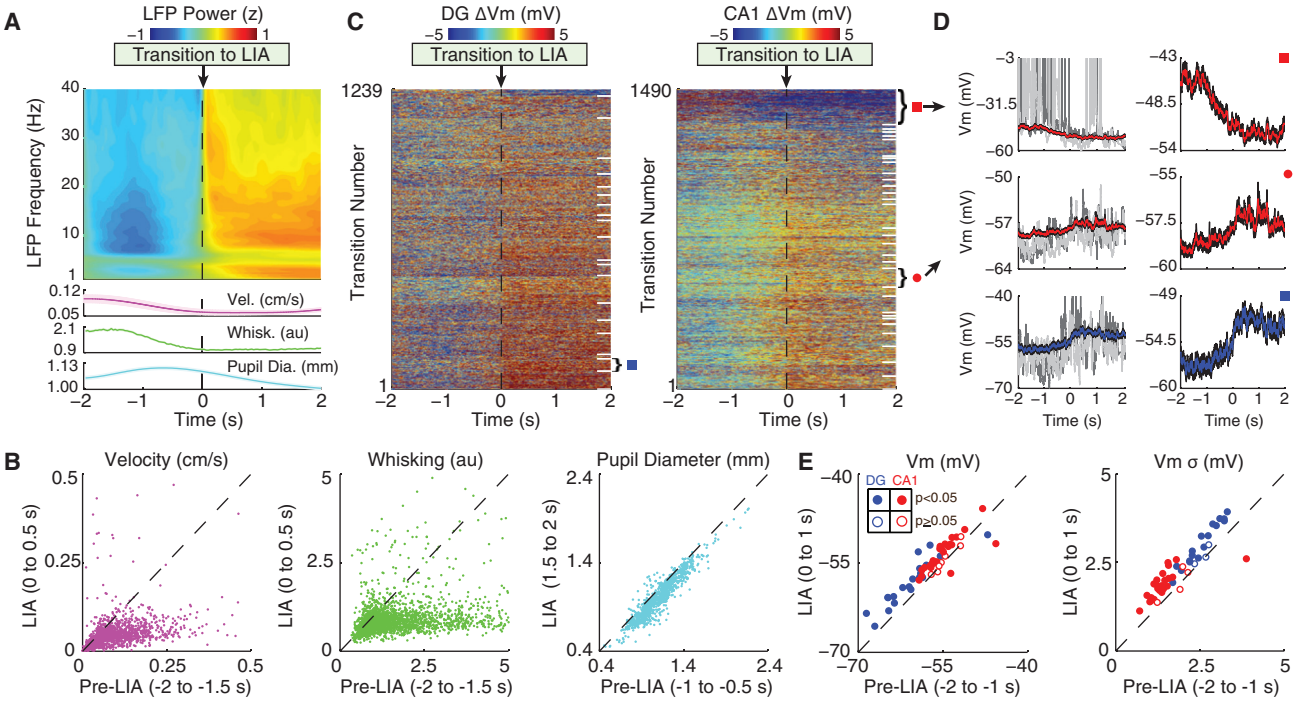

Figure 2. LIA Is Associated with a Depolarized Membrane Potential and Large Subthreshold Fluctuations

(A) Top panel shows a spectrogram of the average LFP power (*Z* score by frequency) triggered on transitions to LIA, which occur at time 0. Bottom panels show the average velocity (Vel.), whisking (Whisk.), and pupil diameter (Pupil Dia.) (shaded regions mark mean ± SEM). Note that transitions to LIA were associated with an increase in delta (0.5–3.5 Hz) and beta (10–20 Hz) LFP power.

(B) Scatterplots of median velocity, whisking, and pupil diameter before (Pre-LIA) and after the transition (LIA). Each point comes from a single transition. The axis labels list the time windows used for computing median values. Locomotor velocity (n = 2,729 transitions), whisking (n = 2,695 transitions), and pupil diameter (n = 973 transitions) all showed a significant decrease across transitions to LIA ($p < 0.001$, Wilcoxon signed-rank tests).

(C) Left panel shows the membrane potential of granule cells triggered on transitions to LIA. Each row corresponds to a single transition, with Vm normalized by subtracting the mean from −2 to 0 s. White lines on the right separate different single neurons. The rows were sorted by each neuron's average Vm change during transitions to LIA. The right panel shows the same for CA1 pyramidal neurons.

(D) The top left panel shows the average Vm in red (black shaded region marks mean ± SEM) triggered on transitions to LIA for a single neuron marked by the red square in (C). Grey Vm traces come from two example transitions. The top right panel shows the average Vm from the same neuron but zoomed in to better illustrate the change occurring during LIA transitions. Two other example neurons are shown below.

(E) The left panel shows a scatterplot of mean Vm before (Pre-LIA) versus after (LIA) transitions to LIA. Each point is the average from a single neuron. Dentate granule cells are colored blue, with filled circles marking neurons with significant changes in Vm. CA1 pyramidal neuron averages are marked in red. Similarly, the right panel shows the mean SD of the Vm (high-pass filtered above 5 Hz) before and after transitions to LIA. Axis labels list the time windows used for computing means.

During transitions to LIA, most hippocampal neurons depolarized, and the amplitude of their subthreshold fluctuations increased (Figure 2). To assess the significance of these changes, we compared the average Vm before and after transitions to LIA for each neuron individually. Most neurons significantly depolarized during transitions to LIA (n = 19/20 DG; n = 22/31 CA1), and a small subset significantly hyperpolarized (for DG, n = 1/20; for CA1, n = 2/31; $p < 0.05$, Wilcoxon signed-rank tests). In order to assess the magnitude of subthreshold fluctuations, we first computed the SD of the membrane potential regardless of brain state. By this measure, granule cells had a larger total Vm variability (6.3 mV ± 0.9 mV) than CA1 pyramidal neurons had (4.7 mV ± 0.6 mV), but these values include contributions from state-dependent shifts in the average Vm, in addition to subthreshold fluctuations. To isolate the subthreshold fluctuations from slower changes in the average Vm, we high-pass filtered the membrane potential and compared the SD of the filtered trace before and after transitions to LIA. Similar to the average Vm, most neurons showed a significant increase in Vm variability after transitions to LIA (for DG, n = 17/20; for CA1, n = 25/31), while one showed a significant decrease (for DG, n = 0/20; for CA1, n = 1/31; $p < 0.05$, Wilcoxon signed-rank tests). We also found notable differences between CA1 pyramidal neurons and DG granule cells. Specifically, during LIA, dentate granule cells were more hyperpolarized and had larger Vm fluctuations (Vm = −58.1 mV ± 0.9 mV; σ = 3.0 mV ± 0.1 mV) compared to CA1 pyramidal cells (Vm = −53.6 mV ± 0.5 mV; σ = 1.9 mV ± 0.1 mV; $p < 0.001$). Across transitions to LIA, granule cells depolarized more than CA1 pyramidal neurons (DG ΔVm = 2.5 mV ± 0.5 mV; CA1 ΔVm = 1.2 mV ± 0.3 mV; $p < 0.05$), with a similar increase in Vm variability (DG Δσ = 0.4 mV ± 0.05 mV; CA1 Δσ = 0.4 mV ± 0.07 mV; p = 0.60, Mann-Whitney U tests).

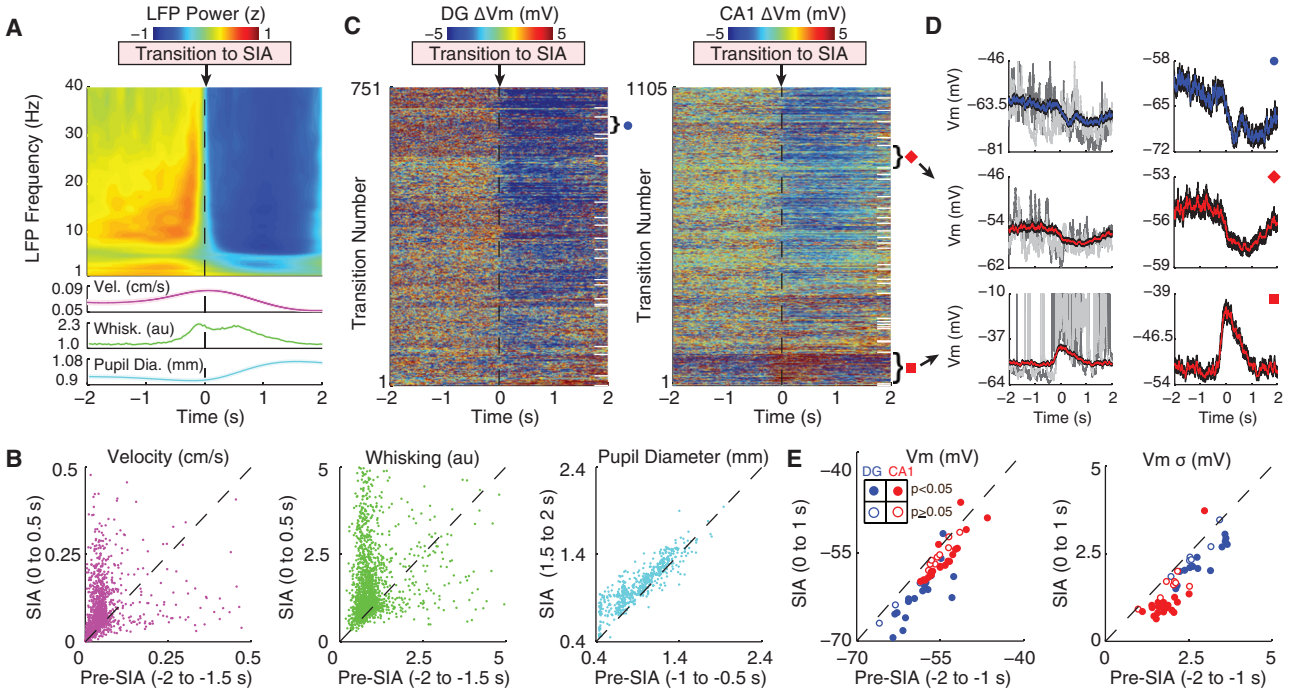

Figure 3. SIA Is Associated with a Hyperpolarized Membrane Potential and Small Subthreshold Fluctuations

(A) The top panel shows a spectrogram of the average LFP power (*Z* score by frequency) triggered on transitions to SIA, which occur at time 0. The bottom panels show the average velocity (Vel.), whisking (Whisk.), and pupil diameter (Pupil Dia.) (shaded regions mark mean ± SEM). Note that transitions to SIA are associated with a broadband decrease in LFP power.

(B) Scatterplots of median velocity, whisking, and pupil diameter before (Pre-SIA) compared to after (SIA) the transition. Each point comes from a single transition, and axis labels list the time windows used for computing median values. Locomotor velocity (n = 1,856 transitions, mostly reflecting postural adjustments), whisking (n = 1,825 transitions), and pupil diameter (n = 558 transitions) all showed a significant increase across transition to SIA ($p < 0.001$, Wilcoxon signed-rank tests).

(C) The left panel shows the membrane potential of granule cells triggered on transitions to SIA. Each row corresponds to a single transition, and Vm was normalized by subtracting the mean from −2 to 0 s. White lines on the right separate different single neurons. The rows were sorted by each neuron's average Vm change during transitions to SIA. The right panel shows the same for CA1 pyramidal neurons.

(D) The top left panel shows the average Vm in blue (black shaded region marks mean ± SEM) triggered on transitions to SIA for a single neuron marked by the blue circle in (C). Gray Vm traces come from two example transitions. The top right panel shows the average Vm from the same neuron but zoomed in to better illustrate the change occurring during SIA transitions. Two other example neurons are shown below.

(E) The left panel shows a scatterplot of the mean Vm before (Pre-SIA) compared to after (SIA) transitions to SIA. Each point is the average from a single neuron. Dentate granule cells are colored blue, with filled circles marking neurons with significant changes in Vm. CA1 pyramidal neuron averages are marked in red. Similarly, the right panel shows the mean SD of the Vm (high-pass filtered above 5 Hz) before and after transitions to SIA. Axis labels list the time windows used for computing means.

See also Figure S2.

Changes in Vm across transitions to SIA were largely opposite to those associated with transitions to LIA (Figure 3). Overall, most neurons significantly hyperpolarized across transitions to SIA (for DG, n = 17/20; for CA1, n = 20/31), but a few significantly depolarized (for DG, n = 1/20; for CA1, n = 2/31; $p < 0.05$, Wilcoxon signed-rank tests). Similarly, most neurons showed a significant decrease in Vm variability (for DG, n = 14/20; for CA1, n = 22/31; $p < 0.05$). During SIA, dentate granule cells were more hyperpolarized and had larger Vm fluctuations (Vm = −62.5 mV ± 1.0 mV; σ = 2.4 mV ± 0.1 mV) compared to CA1 pyramidal neurons (Vm = −55.9 mV ± 0.6 mV; σ = 1.2 mV ± 0.1 mV; $p < 0.001$). Across transitions to SIA, dentate granule cells hyperpolarized more than CA1 pyramidal neurons did (DG ΔVm = −3.3 mV ± 0.6 mV; CA1 ΔVm = −1.2 mV ± 0.3 mV; $p < 0.002$), with a similar decrease in Vm variability (DG Δσ = −0.5 mV ± 0.07 mV; CA1 Δσ = −0.6 mV ± 0.07 mV; $p = 0.13$, Mann-Whitney U tests). In addition, the more a neuron hyperpolarized across transitions to SIA, the more it tended to depolarize across transitions to LIA ($R^2 = 0.78$, $p < 0.001$; Figure S2C).

While transitions to theta were associated with an increase in locomotor velocity, whisking, and pupil diameter, there were no significant changes in Vm or its variability across the transitions (Figure S2A). Since theta periods tended to occur away from identified LIA and SIA epochs, the resting Vm and the amplitude of subthreshold fluctuations during theta may still be quite different from those of LIA and SIA. To assess this, we compared these quantities for the subset of dentate granule cells (n = 14/20) and CA1 pyramidal neurons (n = 25/31) that we recorded during all three states (LIA, SIA, and theta). As shown in Figure 4A, most neurons were more depolarized during LIA and theta compared to SIA and tended to be

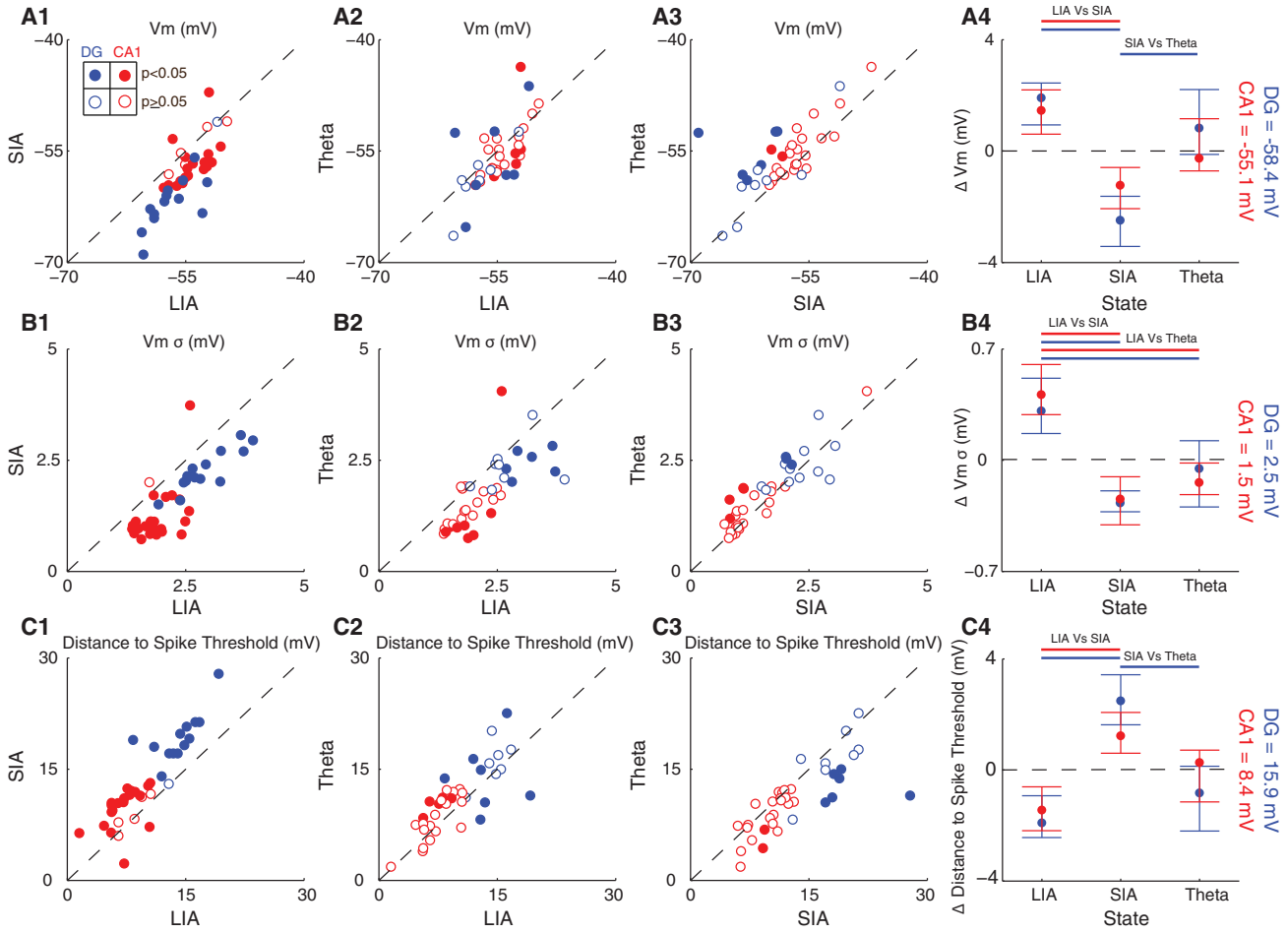

Figure 4. Vm Mean, Variability, and Distance to Threshold Are State Dependent

(A1–A4) In (A1), a scatterplot showing the average Vm during LIA compared to SIA. Each point is the average from a single neuron. Dentate granule cells are colored in blue, with filled circles marking neurons with significant changes in Vm. CA1 pyramidal neuron averages are marked in red. (A2) Same as in A1 but comparing LIA and theta. (A3) Same as in A1 but comparing SIA and theta. (A4) Circles mark each state's Vm (median across neurons) after subtracting the mean Vm across states (the dotted line marking zero; absolute value reported on right) for dentate granule cells (blue) and CA1 pyramidal neurons (red). The whiskers mark the 25th and 75th percentiles. Bars above indicate significant differences ($p < 0.05$) using a Mann-Whitney U test.

(B) Same as in (A) but for Vm variability.

(C) Same as in (A) but for distance to spike threshold. The distance to spike threshold was computed as the average spike threshold across LIA, SIA, and theta epochs minus the membrane potential from each state.

more depolarized during LIA than theta. Similarly, Vm variability was significantly larger during LIA, compared to theta and SIA, and tended to be higher during theta than SIA (Figure 4B). Because the behavioral level of arousal increases from LIA to SIA to theta, these results demonstrate that hippocampal subthreshold activity is an approximately U-shaped function of arousal.

Such modulations in resting membrane potential and the amplitude of subthreshold fluctuations may affect the amount of depolarization needed to bring neurons to spike threshold. To measure this, we subtracted each neuron's average spike threshold, which did not depend on brain state, from its state-specific average membrane potential. As shown in Figure 4C, most hippocampal principal cells were significantly closer to spike threshold during LIA compared to SIA and tended to be closer during theta than SIA. In addition, the spike threshold of dentate granule cells (−42.3 mV ± 0.6 mV) was significantly more positive than that of CA1 pyramidal neurons (−46.3 mV ± 0.6 mV; $p < 0.002$, Mann-Whitney U test). Due to their higher spike threshold and hyperpolarized resting membrane potential, dentate granule cells were two times farther from spike threshold compared to CA1 pyramidal neurons during LIA, SIA, and theta, which likely explains the sparse activity of granule cells in vivo. Together, these results indicate how coordinated modulations of membrane potential statistics may contribute to state-dependent network activity by controlling the amount of depolarization needed to bring neurons to spike threshold.

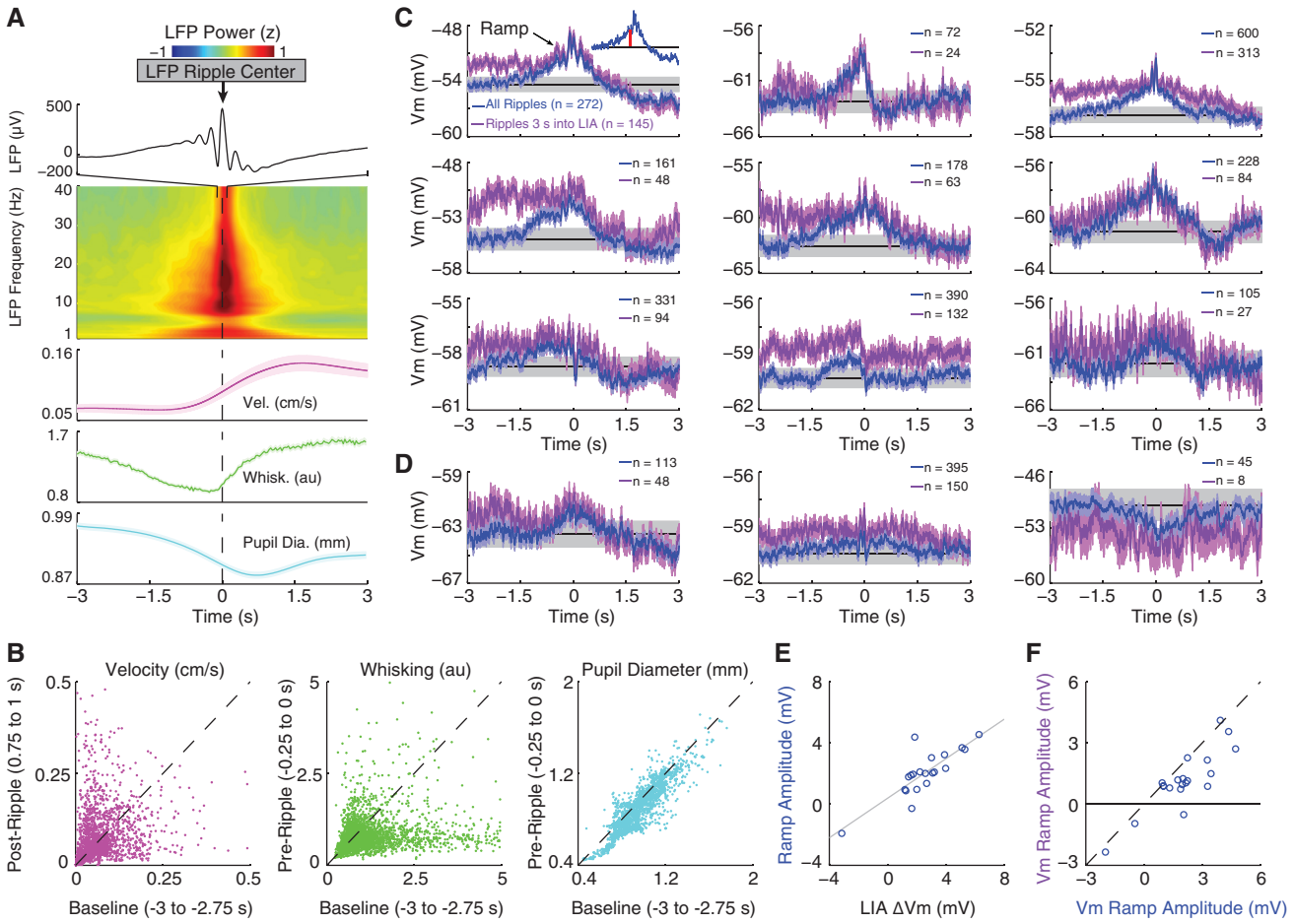

Figure 5. Transitions to LIA Contribute to Pre-ripple Ramps in the Membrane Potential.

(A) The top panel displays the average ripple-triggered LFP from −100 to 100 ms showing the average ripple in the CA1 cell layer. The middle panel shows the average LFP power (*Z* score by frequency) from −3 s to 3 s triggered on ripples, which occur at time 0. The bottom panels show the average velocity (Vel.), whisking (Whisk.), and pupil diameter (Pupil Dia.) around ripple onset (shaded regions mark mean ± SEM).

(B) Scatterplots of median velocity before (Baseline) compared to after (Post-Ripple) ripples and whisking and pupil diameter well before (Baseline) compared to just before (Pre-Ripple) ripples. Each point comes from a single ripple and the axis labels list the time windows used for computing median values. Ripples were preceded by a significant decline in whisking activity (n = 3,705 ripples) and pupil diameter (n = 1,835 ripples; $p < 0.001$, Wilcoxon signed-rank tests).

(C) Ripple-triggered averages of the subthreshold Vm for individual dentate granule cells that show significant pre-ripple ramps (blue). The average Vm using only ripples occurring 3 s into an LIA epoch are shown in purple. Blue and purple shaded regions mark the 95% confidence intervals for each sample. The gray band marks the mean confidence intervals of the pre-ripple Vm (from −3 to −2 s) using all ripples (from the blue trace). The average Vm from this same interval is marked by the black line. The number of ripples entering each average is reported in the legends. The inset illustrates how ramp amplitude (red bar) was computed.

(D) Same as in (C) but for three neurons showing smaller ramps that were not statistically significant.

(E) Scatterplot of the amount each granule cell depolarizes during transitions to LIA (x axis) versus the amplitude of its ramp (y axis).

(F) Scatterplot showing the amplitude of the ramps using all ripples (x axis) compared to using only ripples occurring greater than 3 s into an LIA epoch (y axis).

See also Figure S3.

Origins of Pre-ripple Ramps in the Membrane Potential of Hippocampal Neurons

In a previous study, we found that a subset of CA1 pyramidal neurons (n = 5/30) shows depolarizing and hyperpolarizing ramps in their Vm starting approximately 1 s before ripple onset (Hulse et al., 2016). Can changes in membrane potential associated with transitions to LIA contribute to these ramps? To assess this, we first triggered the LFP and behavioral measures of arousal on ripples detected in the CA1 pyramidal cell layer (Figure 5A). Consistent with SWRs preferentially occurring during the LIA state (Figure S3A), delta and beta power in the hippocampal LFP were high around ripples, while whisking activity and pupil diameter showed a significant decline preceding SWRs (Figures 5A and 5B). Furthermore, 48% of SWRs occurred within 3 s following transitions to LIA (Figure S3B). These findings demonstrate that transitions to LIA are indeed a factor contributing to pre-ripple ramps in the Vm. They also make two specific predictions. First, similar ramps should be present in DG granule cells, since these cells also depolarize across transitions to LIA. Indeed, half of the dentate granule cells showed significant

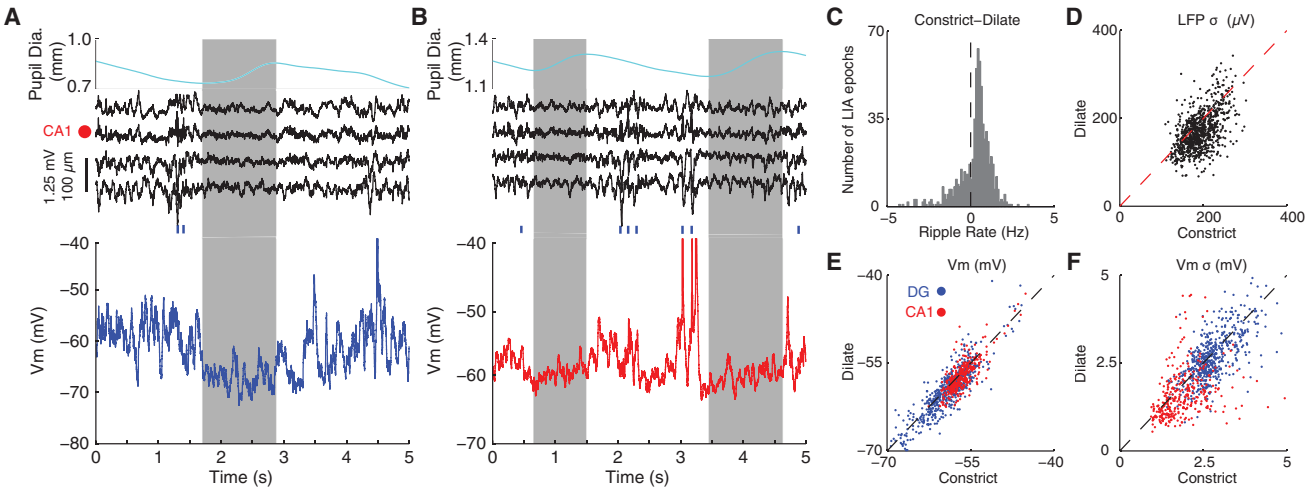

Figure 6. Fluctuations in Pupil Diameter during LIA Are Reflected in the Subthreshold Dynamics of Individual Neurons

(A) Example of correlated changes in pupil diameter (Pupil Dia.), LFPs, and subthreshold activity during a period of LIA. The top panel shows pupil diameter, with the gray box marking the period of dilation. The middle panel shows four LFPs around the CA1 cell layer (marked by red dot). Blue ticks indicate time of ripple occurrence. The bottom panel shows subthreshold activity from a dentate granule cell. Notice that pupil dilation is associated with a flattening of the LFP and a hyperpolarized Vm with low variability.

(B) Same as in (A) but for a period of LIA with two dilation periods and subthreshold activity from a CA1 pyramidal cell.

(C) Histogram showing the difference in ripple rates for constriction (Constrict) compared to dilation (Dilate) across LIA epochs. Positive values indicate a higher ripple rate during constriction relative to dilation. Epochs of LIA with no ripples were excluded. Periods of pupil dilation had significantly lower ripple rates (n = 855 LIA epochs; $p < 0.001$).

(D) Scatterplot showing the SD of the LFP from the stratum radiatum of CA1 (bottom LFP channel in A/B), where sharp waves occur, during periods of constriction compared to periods of dilation. Each dot represents one LIA epoch. Periods of pupil dilation had significantly smaller LFP fluctuations (n = 855 LIA epochs; $p < 0.007$).

(E) Scatterplot showing the average Vm in LIA during periods of constriction compared to periods of dilation. Each dot represents one LIA epoch, and dots are color coded by cell type (blue for DG; red for CA1). Periods of pupil dilation were associated with significantly more hyperpolarized Vm (DG: n = 10 granule cells from n = 539 LIA epochs, $p < 0.007$; CA1: n = 9 CA1 pyramidal neuron from n = 319 LIA epochs, $p < 0.001$).

(F) Same as in (E) but for the SD of the Vm. Periods of pupil dilation had significantly smaller Vm fluctuations (DG: n = 10 granule cells from n = 539 LIA epochs, $p < 0.001$; CA1: n = 9 CA1 pyramidal cells from n = 319 LIA epochs, $p < 0.001$; p values are from Wilcoxon signed-rank tests).

depolarizing ramps in their pre-ripple Vm, and while not statistically significant, many others showed smaller ramps (Figures 5C and 5D). Second, the magnitude of the ramps should correlate with the change in membrane potential associated with LIA transitions. Indeed, neurons that depolarized more across transitions to LIA had larger depolarizing ramps, both in the dentate gyrus (Figure 5E; $R^2 = 0.7$, $p < 0.001$) and in the area CA1 (Figure S3E; $R^2 = 0.66$, $p < 0.001$).

Are transitions to LIA the sole driver of pre-ripple ramps? To answer this question, we restricted our analysis to ripples occurring at least 3 s into a period of LIA (Figure S3). Interestingly, both whisking and pupil diameter still showed significant declines preceding ripples (Figure S3D), suggesting that arousal decreases leading up to ripples even within the LIA state. In addition, though smaller, Vm ramps were still observed for ripples occurring at least 3 s into a period of LIA (Figure 5F). These findings suggest that a reduction in arousal preceding ripples within LIA epochs also contributes to pre-ripple Vm ramps. Importantly, they also suggest that behavioral state changes within LIA may affect network activity.

While previous studies have largely considered LIA to be a homogeneous state, our results suggest that fluctuations in arousal within LIA may affect network activity. To investigate this directly, we divided LIA epochs into periods when the pupil was constricting (72.2% of time) or dilating (27.8% of time) and compared ripple rate, the amplitude of LFP fluctuations, mean Vm, and the amplitude of Vm fluctuations (Figure 6). Figure 6A shows a clear example in which a brief microdilation during an LIA epoch is associated with a desynchronization of the LFP and a hyperpolarization and reduction in Vm variability. Consistent with this example, periods of pupil dilation during LIA had significantly lower ripple rates, lower amplitude LFP fluctuations, a more hyperpolarized Vm, and smaller amplitude Vm fluctuations (Figures 6C–6F). These results demonstrate that LIA is not a homogeneous state. Instead, constant fluctuations in the level of arousal drive changes in subthreshold dynamics and network activity.

DISCUSSION

By combining in vivo whole-cell recordings from identified dentate granule cells and CA1 pyramidal neurons with multisite LFP and behavioral measurements in awake mice, we characterized how hippocampal subthreshold activity is modulated by brain and behavioral state. We show that the membrane potential of most hippocampal neurons is depolarized and has large amplitude fluctuations during LIA. In contrast, SIA is associated with a hyperpolarized membrane potential and smaller

subthreshold fluctuations. During theta oscillations, the Vm has intermediate levels of depolarization and subthreshold fluctuations. In agreement with these changes, the distance to spike threshold depends upon the state of the network. In addition, many hippocampal cells begin to depolarize approximately 1 s before ripple onset. These Vm ramps correlate with brain state transitions to LIA as well as smaller fluctuations in arousal within sustained periods of LIA. Finally, our results provide evidence that rapid fluctuations in pupil diameter during periods of LIA mirror modulations in ripple rate and subthreshold activity.

Previous studies in neocortex have observed state-dependent modulations in subthreshold activity, but the nature of the effects depends upon the brain area and cell type investigated. To account for these findings in neocortex, three models have been proposed: the binary, sigmoidal, and U models (McGinley et al., 2015b). Our results suggest that Vm and its variability are approximately U-shaped functions of arousal at the input (dentate gyrus) and output (area CA1) stages of the hippocampal formation.

However, we found a subset of hippocampal neurons (approximately two CA1 pyramidal neurons and one granule cell) that shows the opposite trend. These neurons tend to hyperpolarize across transitions to LIA (Figure 2), depolarize across transitions to SIA (Figure 3), and hyperpolarize around ripples (Figures 5E and S3E). The activity of these neurons is consistent with that reported in previous studies that have described a subset of principal neurons showing a robust increase in activity during SIA that may code for spatial position in the absence of locomotion and associated theta oscillations (Jarosiewicz et al., 2002; Jarosiewicz and Skaggs, 2004a, 2004b; Kay et al., 2016).

The statistics of the Vm reflect a combination of synaptic input patterns and single-cell properties. There is a wealth of evidence from extracellular recordings that spiking patterns, both within the hippocampus and its input areas, strongly depend on brain state (O'Keefe, 1976; O'Keefe and Nadel, 1978; Buzsáki et al., 1983; Wilson and McNaughton, 1994; Chrobak and Buzsáki, 1996; Jarosiewicz et al., 2002; Lee and Wilson, 2002; Hafting et al., 2005; Foster and Wilson, 2006; Kay et al., 2016; Ólafsdóttir et al., 2016). Furthermore, previous studies have suggested that single-cell properties, such as membrane conductances or synaptic efficacy, may also be modulated by brain state (Winson and Abzug, 1977, 1978; Hasselmo, 1999). However, these properties have been much harder to study in vivo. Our results provide evidence that, in addition to input patterns, single-cell properties are, indeed, modulated by brain state, altering the characteristics of hippocampal neurons.

In particular, the gradual membrane potential depolarization starting approximately 1 s before ripple onset in both dentate granule cells and CA1 pyramidal neurons is difficult to account for based on the known firing properties of hippocampal neurons around ripples (O'Keefe and Nadel, 1978; Buzsáki, 1986; Buzsáki et al., 1992; Wilson and McNaughton, 1994). The predominant view is that the major source of excitatory drive during ripples is the firing of CA3 pyramidal cells (Buzsáki, 2015). While the spiking properties of these neurons have been extensively studied (Csicsvari et al., 2000), there is no evidence that activity in CA3 ramps up as early as 1 s before ripples. In fact, there is no evidence indicating that the spiking output of any excitatory or inhibitory neuron within the hippocampal formation can be the source of synaptic input accounting for the pre-ripple ramps in the membrane potential.

Instead, the observed Vm ramps most likely reflect shifts in the properties of single hippocampal neurons, presumably mediated by state-dependent changes in the neuromodulatory environment (Kalén et al., 1989; Kametani and Kawamura, 1990; Park et al., 1999; Lee and Dan, 2012; Marder et al., 2014). There are two observations in our data that support this interpretation. First, the amplitude of each neuron's Vm ramp is highly correlated with its change in average membrane potential across transitions to LIA. Hence, these transitions, which are known to be associated with a shift in the neuromodulatory environment (Marrosu et al., 1995), are a significant factor contributing to Vm ramps. Second, pupil diameter, which reflects fluctuations in brain state and arousal (Reimer et al., 2014; McGinley et al., 2015b), decreases starting approximately 1 s before ripple onset, mirroring the Vm ramps. This suggests that fluctuations in the neuromodulatory environment within LIA may be a second significant factor contributing to Vm ramps. Consistent with this interpretation, a recent study identified a subset of median raphe neurons that ramp down their firing a second or so before ripple onset, representing one potential source of this neuromodulatory influence (Wang et al., 2015).

Since neuromodulators are expected to act globally on the circuit, the resulting coordinated depolarization of most hippocampal neurons may reflect the network entering a regime conducive to ripple generation and transmission. Specifically, the population burst nucleated within CA3 should be able to effectively drive the CA1 network, largely in the absence of entorhinal input. One mechanism that has been suggested to enable this is an increase in the efficacy of the Schaffer collaterals during LIA (Winson and Abzug, 1977, 1978; Hasselmo, 1999; Hasselmo and McGaughy, 2004). The large subthreshold fluctuations that we observed during LIA may reflect this increase in synaptic efficacy. Our results also show that the membrane depolarization associated with LIA brings neurons closer to spike threshold, which represents an additional mechanism that may enable the effective transmission of ripples. We speculate that a depolarized and highly variable membrane potential may support the nucleation of ripples in CA3 by affecting the probability that a subset of neurons is coactive. Shifts toward this regime occur not only during transitions to LIA but also, importantly, during smaller fluctuations in brain state ("microstates") within sustained periods of LIA. Seen in this light, pre-ripple ramps in the membrane potential reflect the network entering a state capable of generating ripples, while the intracellular depolarization and ripple oscillations observed during SWRs reflect mechanisms specific to the generation process (Ylinen et al., 1995; Hulse et al., 2016).

By combining in vivo whole-cell recordings with multisite LFP and behavioral measurements, we show that the subthreshold dynamics of hippocampal neurons are strongly modulated by brain state. These fundamental measurements reveal several features of hippocampal processing. First, the distance to spike threshold is state dependent. This will affect the recruitment of neurons to network patterns by determining the amount of depolarization needed to reach spike threshold. Second, many

hippocampal neurons show depolarizing ramps in their membrane potential starting approximately 1 s before ripple onset. These ramps reflect coordinated shifts in subthreshold activity toward a state conducive for ripple generation. Finally, even within well-characterized brain states such as LIA, rapid fluctuations in arousal mirror modulations in the membrane potential of hippocampal neurons. This suggests that fast modulations of arousal are reflected in coordinated shifts in hippocampal subthreshold activity. These results support a dynamic view of waking brain states, whereby coordinated fluctuations of single-cell properties contribute to the emergence of network patterns in the hippocampus. Furthermore, they provide a basis for future work dissecting the cellular and modulatory mechanisms supporting brain-state-dependent processing in the hippocampus.

EXPERIMENTAL PROCEDURES

Awake, In Vivo Recordings

Male mice (C57BL/6-E; Strain Code 475; Charles River Laboratories) were head-fixed on a spherical treadmill and allowed to run and walk freely. A potentiometer connected to the axis of the treadmill allowed for behavioral readout of locomotor velocity. To measure pupil diameter and whisker movements, the mouse was illuminated with an infrared (850 nm) LED (M850L3, Thorlabs) and imaged with a charge-coupled device (CCD) camera (scA640-70fm, Basler; with a Nikon AF Micro-Nikkor 105-mm f/2.8 lens) positioned 60° from the midline (mouse's left) and 30° down from the horizontal plane (Sakatani and Isa, 2004). To record LFPs, a single-shank, 32-site silicon probe with 100-μm site spacing was inserted in the coronal plane to a depth of 2,600–3,000 μm. The probe was adjusted so that a recording site was positioned in the CA1 pyramidal cell layer for reliably recording LFP ripple oscillations. Whole-cell recording pipettes were filled with an internal solution containing (in millimolar): 115 K-gluconate, 10 KCl, 10 NaCl, 10 HEPES, 0.1 EGTA, 10 Tris-phosphocreatine, 5 KOH, 13.4 biocytin, 5 Mg-ATP, and 0.3 Tris-GTP. The internal solution had an osmolarity of 300 mOsm and a pH of 7.27 at room temperature. The membrane potential was not corrected for the liquid junction potential. Whole-cell recordings were obtained "blind," according to previously described methods (Margrie et al., 2002). Capacitance neutralization was set prior to establishing the gigaohm seal. Access resistance was estimated online by fitting the voltage response to hyperpolarizing current steps. Recordings were aborted when the access resistance exceeded 120 MΩ or the action potential peak dropped below 0 mV. All animal procedures were performed in accordance with NIH guidelines and with the approval of the Caltech Institutional Animal Care and Use Committee.

Brain State Identification

Brain state identification was carried out in four stages. First, the hippocampal LFPs were subdivided in contiguous 500-ms segments and represented as points in a six-dimensional feature space based on their spectral content. Second, a subset of the points was labeled as theta or LIA using a semi-automated approach. Third, these labeled examples were used to initialize a K-means classifier that categorized all segments as LIA, theta, or unlabeled. Fourth, unlabeled segments with low broadband power were categorized as SIA (Figure S1). The length of the window chosen for brain state identification is based on the notion that brain states persist for periods longer than 500 ms.

Quantification and Statistical Analysis of Behavioral Variables and Subthreshold Activity

To quantify the change in behavioral variables and subthreshold activity upon transitions into LIA, SIA, and theta (Figures 2, 3, and S2), we compared the average values in pre- and post-transition time windows. Similarly, to quantify changes in behavioral variables around ripples (Figures 5 and S3), we compared their median activity in time windows that reflect each signal's dynamics around ripples. Wilcoxon signed-rank tests were used to assess significant differences in the aforementioned values. Mann-Whitney U tests were used to assess differences between states for each individual neuron (indicated by fill of circles in Figures 4A1–4A3, 4B1–4B3, and 4C1–4C3), and Wilcoxon signed-rank tests were used to test for significant difference across all neuron averages (Figures 4A4, 4B4, and 4C4).

To assess the significance of pre-ripple ramping in the neuron-averaged, ripple-triggered Vm traces (Figures 5C and 5D), 95% confidence intervals on the subthreshold Vm were constructed at each sample from −3 s to 3 s. Pre-ripple confidence intervals were computed as the average of the upper/lower 95% confidence intervals from −3 to −2 s. Neurons were considered to have significant ramps if their average Vm spent at least 150 ms continuously above or below the 95% baseline confidence intervals at least 100 ms before the ripple.

In order to evaluate the effect of pupil diameter on neuronal activity during LIA (Figure 6), we divided every LIA epoch into periods where the pupil was constricting and periods where the pupil was dilating. LIA epochs that did not contain both periods of constriction and dilation were excluded (31% of LIA epochs). Next, we compared the average ripple rate, LFP amplitude (SD of the LFP from the channel 200 μm below the CA1 pyramidal cell layer, where sharp waves occur), mean subthreshold Vm, and Vm variability for periods of pupil constriction and dilation. Wilcoxon signed-rank tests were used to assess the significance of differences in neuronal activity between pupil states. A more detailed description of all experimental procedures is provided in the Supplemental Information.

SUPPLEMENTAL INFORMATION

Supplemental Information includes Supplemental Experimental Procedures, three figures, and one movie and can be found with this article online at http://dx.doi.org/10.1016/j.celrep.2016.11.084.

AUTHOR CONTRIBUTIONS

B.K.H. and A.G.S. designed the experiments. B.K.H. performed the experiments. B.K.H., E.V.L., and A.G.S. analyzed the data. B.K.H. wrote the analysis programs and generated the figures. B.K.H., E.V.L., and A.G.S. wrote the paper.

ACKNOWLEDGMENTS

We thank Stijn Cassenaer, Koichiro Kajikawa, Maria Papadopoulou, Britton Sauerbrei, and Kevin Shan for helpful discussion and comments on the manuscript; Andreas Hoenselaar and Mike Walsh for help with instrumentation; Lee-Peng Mok for help with immunohistochemistry; and Koichiro Kajikawa for help with dentate experiments. Confocal imaging was performed in the Caltech Biological Imaging Facility with the support of the Caltech Beckman Institute and the Beckman Foundations. This work was supported by the Mathers Foundation, the Moore Foundation, NIH grant 1DP1OD008255/5DP1MH099907, NSF grant IOS-1146871, and the iARPA contract D16PC00003.

Received: July 26, 2016
Revised: November 7, 2016
Accepted: November 30, 2016
Published: January 3, 2017

REFERENCES

Buzsáki, G. (1986). Hippocampal sharp waves: their origin and significance. Brain Res. *398*, 242–252.

Buzsáki, G. (1989). Two-stage model of memory trace formation: a role for "noisy" brain states. Neuroscience *31*, 551–570.

Buzsáki, G. (2015). Hippocampal sharp wave-ripple: A cognitive biomarker for episodic memory and planning. Hippocampus *25*, 1073–1188.

Buzsáki, G., Leung, L.W., and Vanderwolf, C.H. (1983). Cellular bases of hippocampal EEG in the behaving rat. Brain Res. *287*, 139–171.

Buzsáki, G., Horváth, Z., Urioste, R., Hetke, J., and Wise, K. (1992). High-frequency network oscillation in the hippocampus. Science *256*, 1025–1027.

Carr, M.F., Jadhav, S.P., and Frank, L.M. (2011). Hippocampal replay in the awake state: a potential substrate for memory consolidation and retrieval. Nat. Neurosci. *14*, 147–153.

Chrobak, J.J., and Buzsáki, G. (1996). High-frequency oscillations in the output networks of the hippocampal-entorhinal axis of the freely behaving rat. J. Neurosci. *16*, 3056–3066.

Csicsvari, J., Hirase, H., Mamiya, A., and Buzsáki, G. (2000). Ensemble patterns of hippocampal CA3-CA1 neurons during sharp wave-associated population events. Neuron *28*, 585–594.

Diba, K., and Buzsáki, G. (2007). Forward and reverse hippocampal place-cell sequences during ripples. Nat. Neurosci. *10*, 1241–1242.

Foster, D.J., and Wilson, M.A. (2006). Reverse replay of behavioural sequences in hippocampal place cells during the awake state. Nature *440*, 680–683.

Getting, P.A. (1989). Emerging principles governing the operation of neural networks. Annu. Rev. Neurosci. *12*, 185–204.

Hafting, T., Fyhn, M., Molden, S., Moser, M.B., and Moser, E.I. (2005). Microstructure of a spatial map in the entorhinal cortex. Nature *436*, 801–806.

Harris, K.D., and Thiele, A. (2011). Cortical state and attention. Nat. Rev. Neurosci. *12*, 509–523.

Hasselmo, M.E. (1999). Neuromodulation: acetylcholine and memory consolidation. Trends Cogn. Sci. *3*, 351–359.

Hasselmo, M.E., and McGaughy, J. (2004). High acetylcholine levels set circuit dynamics for attention and encoding and low acetylcholine levels set dynamics for consolidation. Prog. Brain Res. *145*, 207–231.

Hess, E.H., and Polt, J.M. (1960). Pupil size as related to interest value of visual stimuli. Science *132*, 349–350.

Hess, E.H., and Polt, J.M. (1964). Pupil size in relation to mental activity during simple problem-solving. Science *143*, 1190–1192.

Hulse, B.K., Moreaux, L.C., Lubenov, E.V., and Siapas, A.G. (2016). Membrane potential dynamics of CA1 pyramidal neurons during hippocampal ripples in awake mice. Neuron *89*, 800–813.

Jarosiewicz, B., and Skaggs, W.E. (2004a). Hippocampal place cells are not controlled by visual input during the small irregular activity state in the rat. J. Neurosci. *24*, 5070–5077.

Jarosiewicz, B., and Skaggs, W.E. (2004b). Level of arousal during the small irregular activity state in the rat hippocampal EEG. J. Neurophysiol. *91*, 2649–2657.

Jarosiewicz, B., McNaughton, B.L., and Skaggs, W.E. (2002). Hippocampal population activity during the small-amplitude irregular activity state in the rat. J. Neurosci. *22*, 1373–1384.

Kalén, P., Rosegren, E., Lindvall, O., and Björklund, A. (1989). Hippocampal noradrenaline and serotonin release over 24 hours as measured by the dialysis technique in freely moving rats: correlation to behavioural activity state, effect of handling and tail-pinch. Eur. J. Neurosci. *1*, 181–188.

Kametani, H., and Kawamura, H. (1990). Alterations in acetylcholine release in the rat hippocampus during sleep-wakefulness detected by intracerebral dialysis. Life Sci. *47*, 421–426.

Katona, L., Lapray, D., Viney, T.J., Oulhaj, A., Borhegyi, Z., Micklem, B.R., Klausberger, T., and Somogyi, P. (2014). Sleep and movement differentiates actions of two types of somatostatin-expressing GABAergic interneuron in rat hippocampus. Neuron *82*, 872–886.

Kay, K., Sosa, M., Chung, J.E., Karlsson, M.P., Larkin, M.C., and Frank, L.M. (2016). A hippocampal network for spatial coding during immobility and sleep. Nature *531*, 185–190.

Kristjansson, S.D., Stern, J.A., Brown, T.B., and Rohrbaugh, J.W. (2009). Detecting phasic lapses in alertness using pupillometric measures. Appl. Ergon. *40*, 978–986.

Lapray, D., Lasztoczi, B., Lagler, M., Viney, T.J., Katona, L., Valenti, O., Hartwich, K., Borhegyi, Z., Somogyi, P., and Klausberger, T. (2012). Behavior-dependent specialization of identified hippocampal interneurons. Nat. Neurosci. *15*, 1265–1271.

Lee, S.H., and Dan, Y. (2012). Neuromodulation of brain states. Neuron *76*, 209–222.

Lee, A.K., and Wilson, M.A. (2002). Memory of sequential experience in the hippocampus during slow wave sleep. Neuron *36*, 1183–1194.

Lubenov, E.V., and Siapas, A.G. (2009). Hippocampal theta oscillations are travelling waves. Nature *459*, 534–539.

Marder, E. (2012). Neuromodulation of neuronal circuits: back to the future. Neuron *76*, 1–11.

Marder, E., O'Leary, T., and Shruti, S. (2014). Neuromodulation of circuits with variable parameters: single neurons and small circuits reveal principles of state-dependent and robust neuromodulation. Annu. Rev. Neurosci. *37*, 329–346.

Margrie, T.W., Brecht, M., and Sakmann, B. (2002). In vivo, low-resistance, whole-cell recordings from neurons in the anaesthetized and awake mammalian brain. Pflugers Arch. *444*, 491–498.

Marrosu, F., Portas, C., Mascia, M.S., Casu, M.A., Fà, M., Giagheddu, M., Imperato, A., and Gessa, G.L. (1995). Microdialysis measurement of cortical and hippocampal acetylcholine release during sleep-wake cycle in freely moving cats. Brain Res. *671*, 329–332.

McGinley, M.J., David, S.V., and McCormick, D.A. (2015a). Cortical membrane potential signature of optimal states for sensory signal detection. Neuron *87*, 179–192.

McGinley, M.J., Vinck, M., Reimer, J., Batista-Brito, R., Zagha, E., Cadwell, C.R., Tolias, A.S., Cardin, J.A., and McCormick, D.A. (2015b). Waking state: rapid variations modulate neural and behavioral responses. Neuron *87*, 1143–1161.

Niell, C.M., and Stryker, M.P. (2010). Modulation of visual responses by behavioral state in mouse visual cortex. Neuron *65*, 472–479.

O'Keefe, J. (1976). Place units in the hippocampus of the freely moving rat. Exp. Neurol. *51*, 78–109.

O'Keefe, J., and Nadel, L. (1978). The Hippocampus as a Cognitive Map (Oxford, England: Oxford University Press).

Ólafsdóttir, H.F., Carpenter, F., and Barry, C. (2016). Coordinated grid and place cell replay during rest. Nat. Neurosci. *19*, 792–794.

Park, S.P., Lopez-Rodriguez, F., Wilson, C.L., Maidment, N., Matsumoto, Y., and Engel, J., Jr. (1999). In vivo microdialysis measures of extracellular serotonin in the rat hippocampus during sleep-wakefulness. Brain Res. *833*, 291–296.

Polack, P.O., Friedman, J., and Golshani, P. (2013). Cellular mechanisms of brain state-dependent gain modulation in visual cortex. Nat. Neurosci. *16*, 1331–1339.

Poulet, J.F., and Petersen, C.C. (2008). Internal brain state regulates membrane potential synchrony in barrel cortex of behaving mice. Nature *454*, 881–885.

Reimer, J., Froudarakis, E., Cadwell, C.R., Yatsenko, D., Denfield, G.H., and Tolias, A.S. (2014). Pupil fluctuations track fast switching of cortical states during quiet wakefulness. Neuron *84*, 355–362.

Reimer, J., McGinley, M.J., Liu, Y., Rodenkirch, C., Wang, Q., McCormick, D.A., and Tolias, A.S. (2016). Pupil fluctuations track rapid changes in adrenergic and cholinergic activity in cortex. Nat. Commun. *7*, 13289.

Sakatani, T., and Isa, T. (2004). PC-based high-speed video-oculography for measuring rapid eye movements in mice. Neurosci. Res. *49*, 123–131.

Schiemann, J., Puggioni, P., Dacre, J., Pelko, M., Domanski, A., van Rossum, M.C., and Duguid, I. (2015). Cellular mechanisms underlying behavioral state-dependent bidirectional modulation of motor cortex output. Cell Rep. *11*, 1319–1330.

Shan, K.Q., Lubenov, E.V., Papadopoulou, M., and Siapas, A.G. (2016). Spatial tuning and brain state account for dorsal hippocampal CA1 activity in a non-spatial learning task. eLife *5*, e14321.

Somogyi, P., Katona, L., Klausberger, T., Lasztóczi, B., and Viney, T.J. (2013). Temporal redistribution of inhibition over neuronal subcellular domains underlies state-dependent rhythmic change of excitability in the hippocampus. Philos. Trans. R. Soc. Lond. B Biol. Sci. *369*, 20120518.

Squire, L.R. (1992). Memory and the hippocampus: a synthesis from findings with rats, monkeys, and humans. Psychol. Rev. *99*, 195–231.

Steriade, M., Timofeev, I., and Grenier, F. (2001). Natural waking and sleep states: a view from inside neocortical neurons. J. Neurophysiol. *85*, 1969–1985.

Vanderwolf, C.H. (1969). Hippocampal electrical activity and voluntary movement in the rat. Electroencephalogr. Clin. Neurophysiol. *26*, 407–418.

Vanderwolf, C.H. (1971). Limbic-diencephalic mechanisms of voluntary movement. Psychol. Rev. *78*, 83–113.

Vinck, M., Batista-Brito, R., Knoblich, U., and Cardin, J.A. (2015). Arousal and locomotion make distinct contributions to cortical activity patterns and visual encoding. Neuron *86*, 740–754.

Vyazovskiy, V.V., Olcese, U., Hanlon, E.C., Nir, Y., Cirelli, C., and Tononi, G. (2011). Local sleep in awake rats. Nature *472*, 443–447.

Wang, D.V., Yau, H.J., Broker, C.J., Tsou, J.H., Bonci, A., and Ikemoto, S. (2015). Mesopontine median raphe regulates hippocampal ripple oscillation and memory consolidation. Nat. Neurosci. *18*, 728–735.

Wilhelm, B., Giedke, H., Lüdtke, H., Bittner, E., Hofmann, A., and Wilhelm, H. (2001). Daytime variations in central nervous system activation measured by a pupillographic sleepiness test. J. Sleep Res. *10*, 1–7.

Wilson, M.A., and McNaughton, B.L. (1994). Reactivation of hippocampal ensemble memories during sleep. Science *265*, 676–679.

Winson, J., and Abzug, C. (1977). Gating of neuronal transmission in the hippocampus: efficacy of transmission varies with behavioral state. Science *196*, 1223–1225.

Winson, J., and Abzug, C. (1978). Dependence upon behavior of neuronal transmission from perforant pathway through entorhinal cortex. Brain Res. *147*, 422–427.

Ylinen, A., Bragin, A., Nádasdy, Z., Jandó, G., Szabó, I., Sik, A., and Buzsáki, G. (1995). Sharp wave-associated high-frequency oscillation (200 Hz) in the intact hippocampus: network and intracellular mechanisms. J. Neurosci. *15*, 30–46.